Proceedings of the 21st ICSMGE, Vienna, Austria, 14 – 19 June 2026. Pistrol, Adam & Schweiger (eds.)
Published by: ÖGG, Austrian Society for Geomechanics, Salzburg, Austria, ISBN 978-3-9503898-4-5
https://doi.org/10.53243/ICSMGE2026-1248

Groundwater and seasonal effects in geosynthetics-reinforced pile-supported embankments: field measurements and 3D experiments

Suzanne J.M. van Eekelen, Rob A. Zwaan
Deltares, Delft, Netherlands, suzanne.vaneekelen@deltares.nl

Adam Bezuijen
Bezuijen Consult, Netherlands

Alain Nancey
Solmax, Bezons Cedex, France

ABSTRACT: This paper investigates the influence of groundwater and seasonal effects on geosynthetic-reinforced pile-supported (GRPS) embankments. The paper presents field measurements in a partly submerged piled embankment, with a fluctuating groundwater level. The seasonal variations in the measured geosynthetic strains closely matches the seasonal temperature changes in the Dutch moderate circumstances with limited frost, but show much less correlation with the fluctuating groundwater levels. In addition, 3D experiments showed that rising groundwater primarily reduces the load, mainly through uplift forces, but also causes a slight reduction in soil arching. However, the soil arching quickly recovers when the groundwater level decreases again. The slight reduction in soil arching does not affect the strain in the geosynthetic reinforcement; both the experiments and the field test do not show a significant correlation between groundwater levels and geosynthetic reinforcement strains. The Concentric Arches (CA) model (CUR226, 2016) provides the most accurate match compared to several other well-known calculation models.

KEYWORDS: Pile-supported embankments, geosynthetic reinforcement, soil arching, groundwater, seasonal effects.

1 INTRODUCTION

Basal-reinforced pile-supported embankments are widely used in areas with soft soils. They consist of a field of piles beneath an embankment. One or more layers of basal reinforcement (BR) are installed at the base of the embankment. In most cases, the basal reinforcement consists of a geosynthetic (GR, van Eekelen and Han, 2020), and in some cases of a steel mesh (SR, Topolnicki et al., 2019, van Eekelen et al., 2024, Schneider et al., 2024). Several countries published design guidelines for the geosynthetic reinforcement, such as EBGEO [1], British Standard BS8006 [2] and CUR226 [3, 4]. Soil arching is the most important phenomenon in these design guidelines, and in all cases, validation of the design methods was done using data obtained in dry embankments, in which the groundwater table is below the embankment.

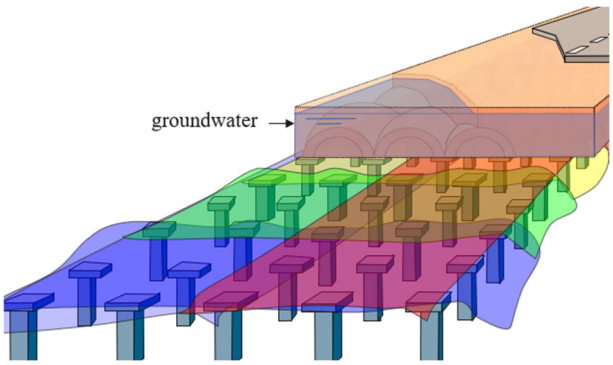

Figure 1. Groundwater in the geosynthetic-reinforced pile-supported (GRPS) embankment.

This paper focuses on the influence of groundwater in the embankment (Figure 1). Limited research was done before on the influence of water in a piled embankment. Briançon and Simon (2012), Sloan (2011), and Van Eekelen et al. (2020) observed that heavy rainfall affects measurements. In these cases, the water or the temperature drop caused by the water may play a role. Song et al. (2018) presented small-scale 2D trapdoor tests with sand and concluded that water can degrade the soil arching. Wang et al. (2019), however, showed with full-scale 3D model experiments that the soil arching strengthened with an increasing water level.

This paper looks at how groundwater in the embankment affects the soil arching and strains in the GR. First, the paper presents results of a field monitoring project that show seasonal effects, and a series of experiments. Then, the paper describes the effect of uplift forces due to water and gives some calculation rules that can be included in several well-known (limit equilibrium) calculation models to include the effect of uplift-forces. Calculation results will be compared with the measurements in the experiments.

2 FIELD STUDY IN THE KRIMPENERWAARD

Van Eekelen et al. (2022, 2023) described a piled embankment built in the polder Krimpenerwaard in the Netherlands (Figure 2 - Figure 4). The new road opened on 6 April 2019. The pile caps measured 0.75 m x 0.75 m and had smooth, rounded edges. They were installed on end-bearing prefab concrete piles with an average centre-to-centre (ctc) spacing of 2.28 m across and 2.27 m along the road axis. This spacing varied locally a few cm.

The basal reinforcement consisted of two layers of woven PET geotextile (TenCate Geolon® 400/50 each).

- The bottom layer was installed across the road axis.
- The top layer was installed parallel to the road axis.

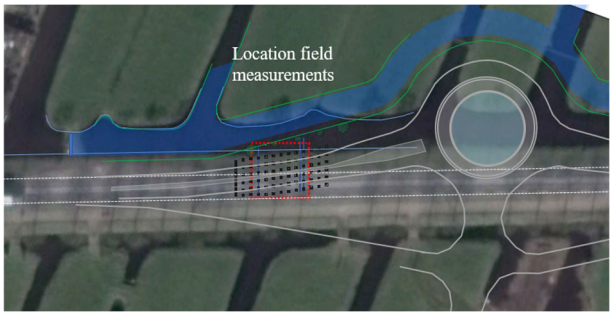

Figure 2. Planned roundabout in a peaty area with the measurement location indicated.

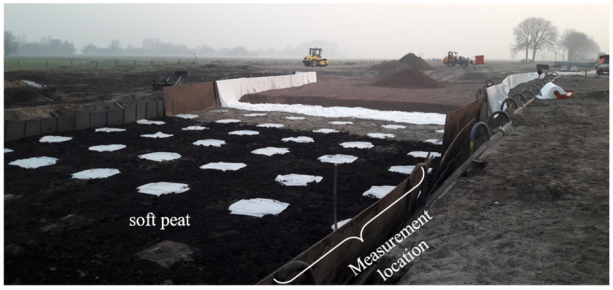

Figure 3. Measurement location

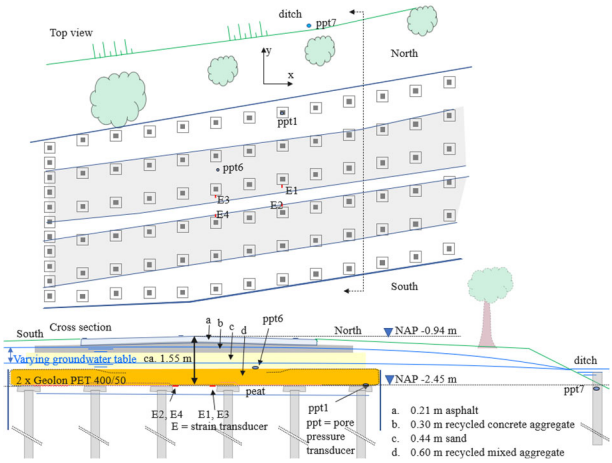

Figure 4. Lay-out of the geotextile-reinforced piled embankment and monitoring equipment. Modified after van Eekelen et al., 2023.

Figure 4 shows the monitoring set-up:

- Strain transducers E1 to E4 measured the geotextile strain.
- Pore pressure transducers ppt1 and ppt6 measured the varying groundwater table.
- Ppt 7 measured the water level in the adjacent ditch.
- The air temperature at the test location was measured hourly.

The load distribution in the embankment was not measured.

3 MODEL EXPERIMENTS WITH GROUNDWATER

A series of experiments was conducted to study how groundwater affects a BRPS embankment. Van Eekelen et al., 2012, 2024 described the tests in more detail. Figure 5 shows the test setup.

A steel plate supported a sealed and water-soaked foam cushion. A tap allowed water to drain from the foam cushion. Four PVC piles (0.1 m diameter) passed through the steel plate.

Two layers of Geolon 100-50 woven geotextile were placed perpendicular to each other, and directly on top of one another. They were attached to a rigid steel frame. Together, they layers had a tensile strength 100+50 = 150 kN/m and a tensile stiffness at 2% strain $J_{2\%}$ = 1200 kN/m and 1013 kN/m for 10 and 1000 hours loading, respectively.

An evenly distributed surcharge load was applied on the fill surface, using a water cushion. A rubber sheet greased with Vaseline minimised the wall-soil friction. Measurements included:

- The load distribution in the fill, using total pressure cells.
- The GR deflection, using a liquid levelling system (water pressure cells in a tube filled with water and connected to a reference box with water).
- The GR strains, using strain cables (van Eekelen et al., 2024).

Two types of mixed demolition waste granulate were used:

- With fines (d/D = 0/31.5 mm).
- Without fines (*d*/D = 4/31.5 mm),

where *d* and *D* were the lower and upper sieve sizes (EN13242, 2015). Table 1 lists the fill details. The values of $\varphi'_{15\%}$ were obtained from four drained large-scale triaxial tests, using samples with a diameter of 0.45 m.

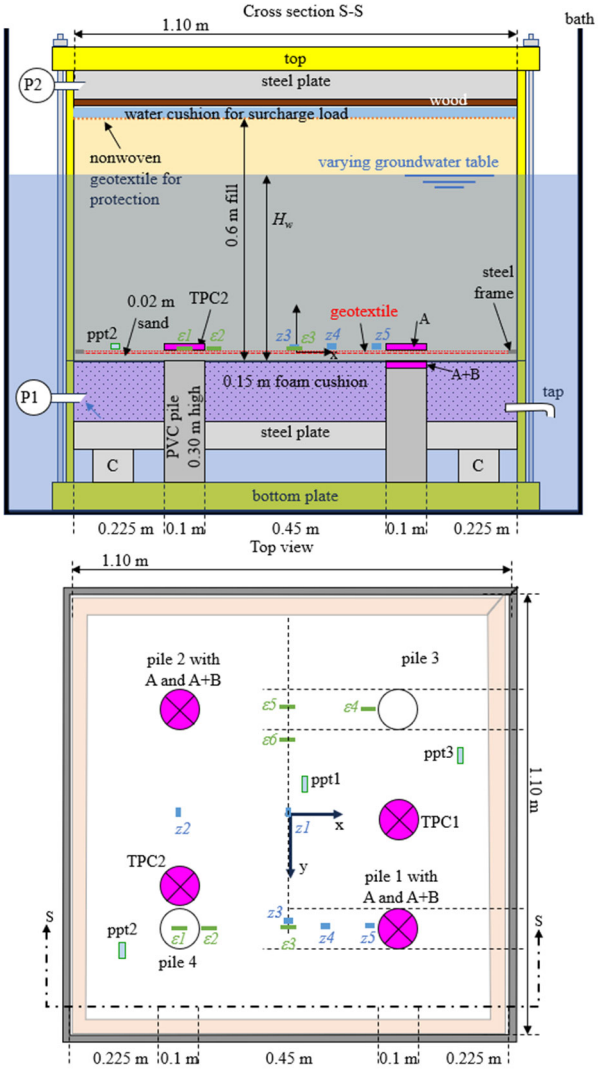

Figure 5. Test setup GRPS embankment with varying groundwater table

Table 1. Test details of the small-scale experiments.

Test no.	1	2	3
Fill height above steel (m)	0.65	0.60	0.60
Limiting sieve sizes *d*/*D* (mm/mm)	4/31.5	0/31.5	4/31.5
Median particle size D_{50} (mm)	18.8	7.0	18.8
Unit weight dry fill γ_d (kN/m^3)	13.19	14.60	13.20
Unit weight saturated fill γ_s (kN/m^3)	18.11	19.00	18.12
Unit weight initial* fill γ_i (kN/m^3)	13.90	15.39	13.91
Porosity n (V_{pores} / V_{total})	0.50	0.45	0.50
Friction angle unsaturated fill $\varphi'_{15\%}$ (°)	41.0	39.4	41.0
Friction angle saturated fill $\varphi'_{15\%}$ (°)	40.5	39.6	40.5

* Partly saturated

After installing the reinforcement, sensors and the fill, the test box was closed and placed in a water bath (Figure 5). The subsoil support was then removed by creating a vacuum in the foam cushion between the piles.

Next, the bath was filled. The groundwater table in the fill followed the water level in the bath easily. In Tests 2 and 3, the groundwater table was later lowered again. After that, the surcharge load was increased in steps. After each surcharge load step, a groundwater cycle was applied again. In Test 1, the phreatic line was kept constant.

Chapter 5 presents and interprets the measurement results from Test 2 and compares them with calculation results.

4 CALCULATIONS

4.1 *European design methods*

The load distribution and geosynthetic strain in GRPS embankments can be calculated using several established methods. The four main European design methods are:

1. The Concentric Arches model by van Eekelen et al., (2013, 2015, adopted in CUR226, 2016).
2. The Zaeske model (2001), adopted in EBGEO, (2011).
3. The Hewlett and Randolph model (1988), adopted in both the French ASIRI (2012) and the British Standard (BS8006, 2010).
4. The modified Marston and Anderson model (1913) as adopted in BS8006, 2010 (van Eekelen et al., 2011).

All four models start by dividing the vertical load into two load parts (Figure 2):

- Part A (kN/pile) – load directly transferred to the piles. This part is relatively large, due to soil arching.
- Part B+C (kN/pile) – residual part that is supported by the subsurface between the piles.

In the second calculation step, the methods calculate the geosynthetic (GR) strain, which implicitly further divides B+C into:

- Part B – Load transported via the geosynthetic towards the piles.
- Part C – Load carried by the subsoil.

In the experiments described in this paper, the foam cushion underneath the GR was sucked vacuum. This removed the subsoil support, so that for all tests the subsoil support was zero, meaning C = 0 for all tests.

The load distribution (measured in the experiments) and the geosynthetic strain (measured in both the experiments and the field test) were calculated using the models mentioned above. No partial factors were applied.

4.2 *Input parameters - Field test*

Table 1 lists the input parameters that were used to simulate the field test. Some remarks:

- Internal friction angle (φ'): For design purposes, the characteristic value of the internal friction angle should be used. However, for comparison with measurements, it is better to use the weighted average value of the average values for the soil layers within the soil arch (van Eekelen & Han, 2020).

  For the well-compacted sand layer, an average value of 35° is a reasonable estimate. The 0.6 m aggregate layer below the sand layer consisted of mixed concrete and masonry granulate, with a high masonry content. The shape of the grains was sub-angular, and the grain distribution was average to good, resulting in an average value of 36.5° to 38.5°. The weighted average for the two layers ranges between 35.8° and 36.9°. In the calculations presented in this paper, the value of 36° was used.
- When comparing to field measurements, traffic load is usually not included in the calculations. In contrast, van Eekelen et al. (2023) also calculated with 25% of the design load, to account for its permanent influence on the traffic load on the geotextile strain. This results in higher calculated geotextile strains. This was not done in this paper for clarity reasons; only the most conservative option of zero traffic load was considered (safe side in model validation).

CUR226 (2016) requests to reduce the soil arching for a piled embankment of this type, with a relatively thin fill and high traffic load. It is assumed that the soil arching reduces permanently due to the on-going traffic load. For the present configuration and traffic load, Table 2.3 of CUR226 prescribes a reduction factor $\kappa = 1.58$. Applying this factor would again result in higher values for the geosynthetic strain. Since EBGEO, ASIRI and BS8006 do not use this factor, and using the factor would result in higher values for the geosynthetic, this factor is not applied in this paper ($\kappa = 1.58$: safe side in model validation).

Table 2. Input values* for the simulation calculations of the field test.

Date	28 Feb 2019	1 Mar 2019	5 Mar 2019	12 Mar 2019	24 Apr 2019	29 Feb 2020	25 Aug 2030
Height fill (m)	0.00	0.30	0.60	1.00	1.51	1.51	1.51
Tensile stiffness geotextile (kN/m)	3200	3200	3200	2961	2722	2544	2426

* and: centre-to-centre distance piles $s_y = s_y = 2.28$ m. The square pile caps width $a = 0.75$ m, unit weight fill $\gamma = 19$ kN/m^3, fill friction angle $\varphi = 36°$, subgrade reaction $k = 0$ kN/m^3, traffic load $p = 0$ kPa, soil arching reduction coefficient κ is 1.0 (no soil arching reduction).

4.3 *Input parameters - Experiments*

Figure 5 gives the geometric properties of the test setup, and Table 1 lists the fill properties. The groundwater table H_w was derived from the measured pore pressures (ppt 1, 2 and 3). The weighted value of the fill unit weight γ, used in equations (2) to (5), was derived from the dry unit weight γ_d below the groundwater level (combined with Archimedes' p_{uplift} for the grains, see next section) and the initial unit weight γ_i (kN/m^3) above groundwater level. The latter includes the 5.4% moisture content of the sand above the phreatic line.

The wall-soil friction R was 20-25% of the total load. This value was obtained by subtracting the measured sum A+B+C from the total effective load. R was then subtracted from the surcharge load. Since there was no subsoil support during the tests, the subgrade reaction was $k = 0$ kN/m^3.

The geotextile tensile stiffness $J_{2\%}$ was selected in line with the test duration, resulting in $J_{2\%} = 1106$ kN/m.

4.4 *Water in the calculations*

Archimedes' principle states that a body immersed in a fluid experiences an upward force equal to the weight of the displaced fluid (Figure 6). This aligns Terzaghi's effective stress definition, in which the effective stress equals the total stress minus the pore pressure.

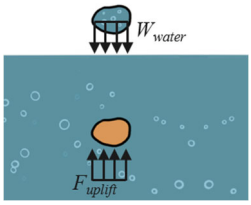

Figure 6. Archimedes' principle; $F_{uplift} = W_{water}$

In the present study, Archimedes' upward pressure (p_{uplift}) is used to account for the effect of water in the fill. It is defined as:

$$p_{uplift} = (1 - n) \cdot H_w \cdot \gamma_w \quad \text{(kPa)} \tag{1}$$

where n (-) is the porosity, H_w (m) is the groundwater table above the piles, and γ_w is the unit weight of water (9.81 kN/m^3). In the Concentric Arches (CA) calculations, p_{uplift} is integrated by reducing surcharge load p with p_{uplift}. In theory, this approach aligns Terzaghi's effective stress principle. However, using the Terzaghi's effective stresses is not possible for the CA model. This is explained below for the CA model (van Eekelen et al., 2013), but also applies for EBGEO.

First, the CA model calculates the load distribution A% and (B+C)%, without including the surcharge load ($p = 0$). This results in $A_{p=0}$ and $(B+C)_{p=0}$. So far, the calculation only uses the soil weight above the arches (besides geometry and material properties). Therefore, using Terzaghi's effective stress-approach would only impact the calculation for the fill part above the arches.

Secondly, the CA model includes the surcharge load:

$$A_{p>0} = \frac{\gamma H + p}{\gamma H} \cdot A_{p=0} \quad \text{and} \tag{2}$$

$$(B + C)_{p>0} = \frac{\gamma H + p}{\gamma H} \cdot (B + C)_{p=0} \tag{3}$$

In this study, the effect of groundwater is included by modifying these equations into:

$$A_{p>0} = \frac{\gamma H + p - p_{uplift}}{\gamma H} \cdot A_{p=0} \quad \text{and} \tag{4}$$

$$(B + C)_{p>0} = \frac{\gamma H + p - p_{uplift}}{\gamma H} \cdot (B + C)_{p=0} \tag{5}$$

5 IMPACT GROUNDWATER AND SEASONAL EFFECTS

5.1 *Geotextile strains in the field test*

In the field test, the load distribution was not measured, but the geotextile strains were. Consequently, the field data can be used to validate the two calculation steps described in Section 4.1 together, but not individually.

Figure 7 compares the measured strains with the measured groundwater table. Strain gauges E1 and E2, located on the east-side, give higher values than the two other strain gauges, E3 and E4, most likely due to a larger pile spacing at the E1/E2 location.

All measured strains show a seasonable pattern: with higher strains in summer than in winter. Each successive summer gives slightly higher strains than the previous one. This gradual increase can be explained by the creep behaviour of the geotextile.

Figure 7 shows no clear correlation between strains and groundwater table. However, Figure 8 shows a strong correlation between strain and seasonal variations in average daily air temperature. The geotextile strain is higher in summer. This field site was in the Netherlands, which has a moderate climate with only a few days of frost per year. In colder climates with severe frost, the behaviour differs.

Gunnvard (2023) presents a two-year monitoring project of a timber pile-supported road embankment in North-Sweden. He showed how frost heave and the subsequent thaw period affected the load distribution and GR strains (Gunnvard 2023, digital pages 180-182). During frost heave, all GR strains and the pressures in the system increased significantly, followed by a partial recovery during and after thawing. This cycle contrasts the one observed in the Netherlands.

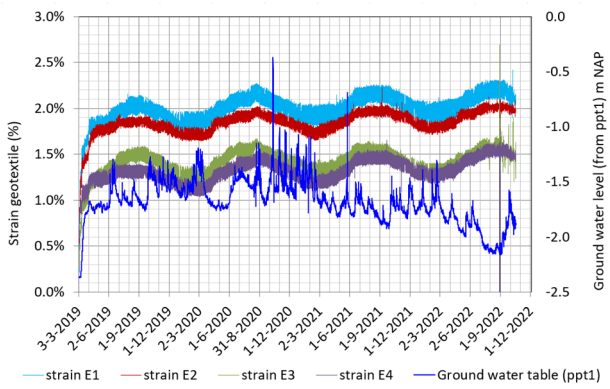

Figure 7. Comparison measured geotextile strains and measured groundwater table (modified after van Eekelen et al., 2023)

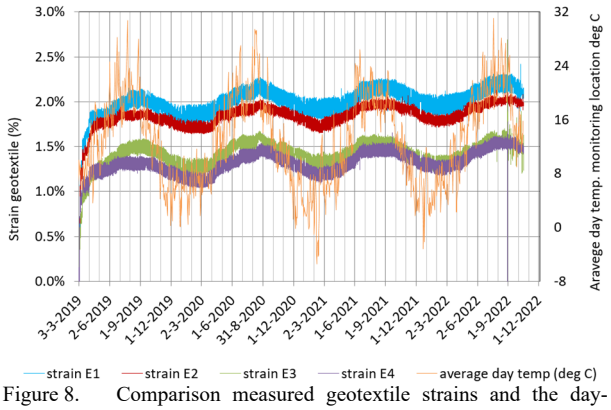

Figure 8. Comparison measured geotextile strains and the day-average of the air temperature which was measured hourly at the field monitoring location (modified after van Eekelen et al., 2023).

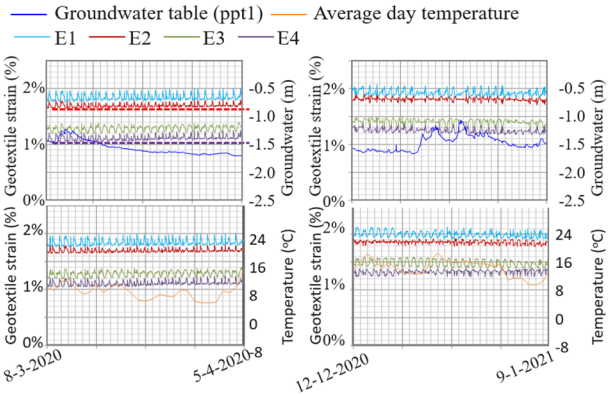

Figure 9. Details of Figure 7 and Figure 8; left: four dry weeks (no rain) and right: a four-week wet period (several rainy periods).

To study short-term effects, Figure 9 zooms in on two four-week-long periods. The left-hand-side graphs show a dry period, without rain, and a decreasing groundwater table. The right-hand-side graphs show a wet period, with rainy periods and an increasing groundwater table. The measured strains show a clear daily cycle, the underlying cause remains unclear. For example Van Eekelen et al. (2007) reported similar daily variations. Possible explanations include the daily cycle of traffic load, or soil temperature (Please note that Figure 9 shows daily averaged temperatures; therefore, no daily cycles appear). However, the peaks did not occur at the same time of the day. The graphs show that rain makes the daily cycle less pronounced. Possibly, this is caused by the relatively constant

and low temperature caused by the rain, which flattens the daily cycle.

Figure 10 compares measured GR strains with calculated values from the Dutch field test. Seasonal and groundwater effects were not included in the calculations. In this case, the CA model match the measured values significantly better than the other calculation models.

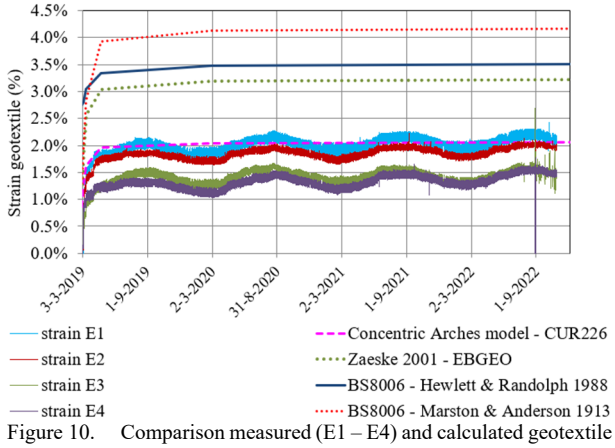

Figure 10. Comparison measured (E1 – E4) and calculated geotextile strains of the field test. Input data calculations in Table 2.

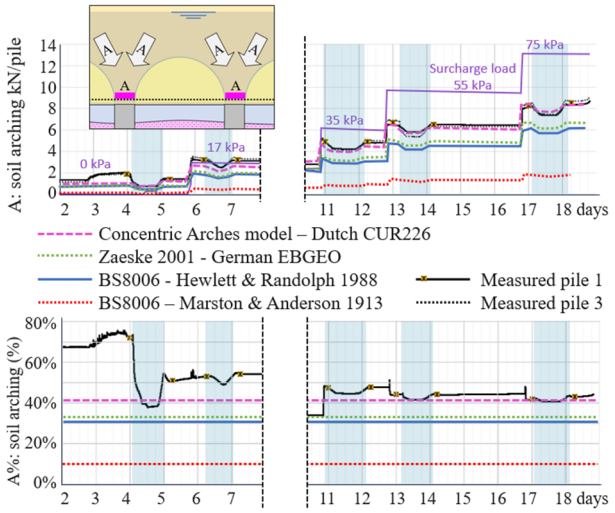

Figure 11. Calculated and measured soil arching (load part A in kN/pile (top) and in % of total load (bottom), for Test 2. Between days 8 and 11, the surcharge load cushion leaked. The blue zones indicate the high-groundwater phases.

5.2 *Soil arching in the experiments*

Figure 11 compares the measured and calculated soil arching, expressed as load part A (kN/pile). In this case, the uplift forces were included in the calculations, as described in Section 4.4. The results show:

- A rising groundwater level gives a limited decrease in soil arching.
- This decrease is mainly due to Archimedes' uplift forces rather than changes in soil arching itself. This is demonstrated by the calculations, which closely match the measurements. The calculations included the Archimedes' uplift but did not reduce the soil arching due to a higher groundwater level.
- The bottom graph in Figure 11 shows a slight decrease in soil arching A% due to groundwater. This indicates that uplift is the dominant mechanism but not the sole contributor.
- The soil arching almost immediately rebounds when the phreatic line decreases. Groundwater cycles caused less than 3.5% change in soil arching, both up and down. The only exception is the first cycle, which reduced arching by 26%. At that stage, the arching had not yet reached equilibrium.

The CA model matches the measurements more closely than EBGEO, Marston and Anderson (1913) and Hewlett and Randolph (1988), all of which underestimate the soil arching in this case.

5.3 *GR strains and deflection in the experiments*

The GR strain was measured using bicycle brake cables, attached to the geotextile with tie wraps. The twisted steel wire was pulled out its outer sleeve by roughly 10 mm and fixed to the geotextile. A displacement transducer registered the relative movement between wire and sleeve. Some recorded strains exceeded rupture levels without actual rupture. This indicates limited quantitative reliability. However, the measured patterns seem qualitatively realistic, as in Figure 12, they match our expectations: the highest GR strains were measured in the strips between adjacent piles. The closer to the pile, the higher the strain. Outside the GR strip between adjacent piles (ε6), we observe much lower strains, typically around zero.

The GR strains showed no significant response to groundwater changes, consistent with the field test results, described in the previous section. Temperature appeared more influential than groundwater level.

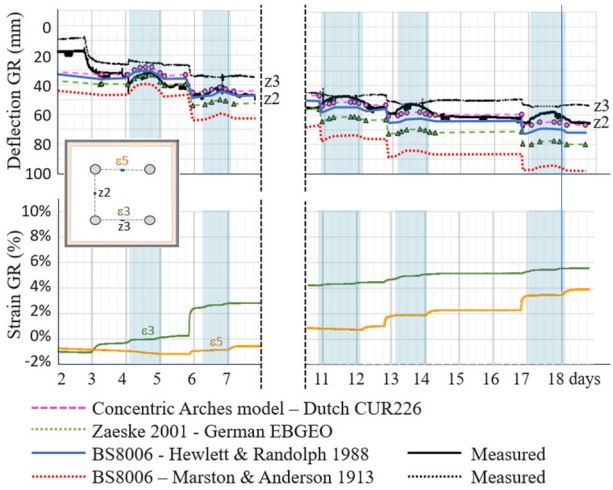

Figure 12. Top: Measured and calculated deflection; bottom: GR strain.

The second graph in Figure 12 compares measured and calculated GR deflection at the midpoint between two piles. The calculations were done for the middle of two adjacent piles. The CA model again matches the measured deflection nicely. Some sensors, specifically z2, show heave during groundwater rise; this effect was also predicted by the calculations, though to a lesser degree.

The response on groundwater rise was similar for both fill types, with and without fines.

6 CONCLUSIONS

A field test and laboratory model experiments were performed to study the impact of groundwater in GRPS embankments. The following conclusions were drawn:

- Groundwater variations had no measurable effect on geosynthetic strains, and therefore, on tensile forces in the geosynthetic. This was observed in both the field test and the experiments.

- Seasonal temperature changes significantly affected the GR strains. In the moderate Dutch climate, strains were higher in summer (this paper), while in cold climates with strong seasonal frost, frost heave can increase the GR strains in winter (Gunnvard, 2023).
- Rising groundwater gives a reduction of load part A (soil arching) mainly due to Archimedes' uplift forces, with a small additional effect from reduced soil arching.
- The soil arching recovered immediately when the groundwater level decreased again.
- The Concentric Arches (CA) model reproduced the measured load reduction closely when uplift forces were included in the calculations. The uplift forces can also be included in other calculation models, like the Zaeske model of EBGEO (2011), Hewlett and Randolph (1988) of BS8006 (2016) and ASIRI (2012) and the modified Marston and Anderson (1913) approach of BS8006.
- The CA model provides a closer match to the measurements in the field test and the experiments than the other considered calculation models, which underestimate the soil arching.
- The response on groundwater rise was similar for both fill types, with and without fines.
- An increase of groundwater gives some heave of the GR, due to the uplift forces. This heave disappears upon lowering the groundwater again.
- The presented experiment and field test did not reveal any significant response of GR strains to changes in groundwater. However, earlier studies, like Briançon and Simon (2012) and van Eekelen et al. (2020), reported deformation and load distribution changes after heavy rain. This is possibly due to accompanying temperature changes resulting from such heavy rain showers, or subsoil swelling from increased water content.

7 ACKNOWLEDGEMENTS

The authors are grateful for the support of Solmax-TenCate, both financially and practically, and the support of the TKI-PPS funding of the Dutch Ministry of Economic Affairs.

8 REFERENCES

Archimedes. (circa 250 BCE). Archimedes' Principle.

ASIRI, 2012. *Recommandations pour la conception, le dimensionnement, l'exécution et le contrôle de l'amélioration des sols de fondation par inclusions rigides*, ISBN: 978-2-85978-462-1. Also available in English: *Recommendations for the design, construction and control of rigid inclusions ground improvements* (2013).

Briançon L and Simon B 2012 Performance of Pile-Supported Embankment over Soft Soil: Full-Scale Experiment. *J. of Geot. and Geoenv. Eng.* 138, 551–561. doi: 10.1061/(ASCE)GT.1943-5606.0000561.

BS8006-1:2010. *Code of practice for strengthened/reinforced soils and other fills*. (BSI, London, UK, 2010) DOI:10.1002/9783433600931.

CUR226, see Van Eekelen & Brugman (2016).

EBGEO 2011. *Recommendations for Design and Analysis for Earth Structures using Geosynthetic Reinforcements*. German Geotechnical Society. DOI:10.1002/9783433600931.

Gunnvard, P. 2023. Timber Pile-Supported Embankments – Arching and Reinforcement. Doctoral Thesis Luleå University of Technology, Luleå, Sweden. ISBN 978-91-8048-244-8.

Hewlett, W.J., and Randolph, M.F. 1988. Analysis of piled embankments. Ground Eng., 21, No. 3, 12–18.

Marston, A., and Anderson, A.O. 1913. The Theory of Loads on Pipes in Ditches and Tests of Cement and Clay Drain Tile and Sewer Pipe, Engineering Experiment Station, Bulletin No. 31, Iowa State College of Agriculture and Mechanic Arts, Ames, Iowa, USA, 181p.

CEN NEN-EN 13242 Ontw. en. 2015. *Aggregates for unbound and hydraulically bound materials for use in civil engineering work and road construction*. NEN, the Royal Netherlands Standardization Institute.

Schneider, M., Hell, M., Pandrea, P., Wittekoek, B., van Eekelen, S.J.M., Topolnicki, M., Makowska, K., Sieńko, R., Zachert, H. 2024. Large-scale test on basal steel-reinforced piled embankments, *Proc. ECSMGE 2024*, Lisbon, Portugal, DOI 10.1201/9781003431749-510

Sloan J A 2011 Column-Supported Embankments: Full-Scale Tests and Design Recommendations PhD Thesis. Virginia Polytechnic Institute and State University, Blacksburg, Virginia, USA.

Song J., Chen K., Li P., Zhang Y., and Sun C. 2018. Soil arching in unsaturated soil with different water table. *Granular Matter* 20, *78*. https://doi.org/10.1007/s10035-018-0849-3.

Topolnicki, M. Sołtys, G., Brzozowski, T. 2019. Performance and modelling of road embankment supported on rigid inclusions and a transfer platform with steel geogrid, *Proc. ECSMGE*, Iceland DOI: 10.32075/17ECSMGE-2019-0811

van Eekelen, S.J.M., Van, M.A. & Bezuijen, A. 2007. The Kyoto Road, a full-scale test. Measurements and calculations. *Proc. of ECSMGE14*, Madrid, Spain 1533-1538.

van Eekelen, S.J.M., Bezuijen, A. and van Tol, A.F. 2011. Analysis and modification of the British Standard BS8006 for the design of piled embankments. *Geot. and Geomemb*. 29 (2011) 345 – 359, https://doi.org/10.1016/j.geotexmem.2011.02.001

van Eekelen, S.J.M., Bezuijen, A., van Tol, A.F. 2013. An analytical model for arching in piled embankments. *Geot. and Geom*. 39, 78-102, (2013) DOI 10.1016/j.geotexmem.2013.07.005.

van Eekelen, S.J.M., Bezuijen, A., van Tol, A.F. 2015. Validation of analytical models for the design of basal reinforced piled embankments, *Geot. and Geom*, 43:1, 56 – 81, (2015a) DOI 10.1016/j.geotexmem.2014.10.002

van Eekelen, S.J.M. and Brugman, M.H.A. Eds., 2016. *Design Guideline Basal Reinforced Piled Embankments (CUR226),* CRC Press, Delft, Netherlands, doi.org/10.1201/9781315389806

van Eekelen, S.J.M., Han, J. 2020. Geosynthetic-reinforced pile-supported embankments: state of the art. *Geosynth. Int*. 27 (2) 112-141, DOI 10.1680/jgein.20.00005

van Eekelen, S.J.M., Zwaan, R.A., Nancey, A., Hazenkamp, M., Jung, Y.H. 2022. Field measurements in a partly submerged woven geotextile-reinforced pile-supported embankment. *Proc. 7th EuroGeo Conference. doi:10.1088/1757-899X/1260/1/012046.*

van Eekelen, S.J.M., Zwaan, R.A., Nancey, A., Hazenkamp, M., Jung, Y.H. 2023. Four years field measurements in a partly submerged woven geotextile-reinforced pile-supported embankment. *Proc. 11th Int. Conf. Geosynthetics (ICG11)*, Rome, Italy.

van Eekelen, S.J.M., Wittekoek, B., Zwaan, R.A., Bezuijen, A., Nancey, A., 2024. Groundwater in geosynthetics-reinforced pile-supported embankments, 3D Experiments. *Proc. ECSMGE24*, Lisbon, Portugal.

van Eekelen, S.J.M., Schneider, M., Hell, M., Wittekoek, B., Makowska, K., Zdanowicz, K., Pandrea, P., Sieńko, R., Schauber, P., Topolnicki, M., Zachert, H. 2024. 3D small-scale tests on steel-reinforced piled embankments, *Proc. ECSMGE*, Lisbon, Portugal, DOI 10.1201/9781003431749-526.

van der Peet, T.C., and van Eekelen, S.J.M. 2014. 3D numerical analysis of basal reinforced piled embankments, *Proc. 10th Int. Conf. on Geosynthetics (ICG10),* Paper no. 112, Berlin, Germany

Wang, H.L., Chen, R.P., Cheng, W., Qi, S. & Cui, Y.J. 2018. Full-scale model study on variations of soil stress in geosynthetic-reinforced pile-supported track bed with water level change and cyclic loading. *Can. Geotech. J.* 56: 60–68 (2019).

Zaeske, D. 2001. *Zur Wirkungsweise von Unbewehrten und Bewehrten Mineralischen Tragschichten über Pfahlartigen Gründungselementen*. PhD Thesis, Schriftenreihe Geotechnik, Universität Gh Kassel, Kassel, Germany. Heft 10 (in German).